Finite Element Study of Concrete-Filled Steel Tubes Using a New Confinement-Sensitive Concrete Compression Model

Mathias Johansson,
Lic. Sc., Research Assistant
Department of Structural Engineering, Concrete Structures, Chalmers University of Technology, SE-41296 Göteborg, Sweden
E-mail: mathias.johansson@ste.chalmers.se

Magnus Åkesson,
Ph. D.
Swedish Meteorological and Hydrological Institute, SE-60176 Norrköping, Sweden
E-mail: magnus.akesson@smhi.se
(Formerly Department of Structural Engineering)

ABSTRACT

The constitutive model in this paper addresses the influence of confinement on the compressive response in concrete structures, which is one issue when dealing with their compressive failure. The elasto-plastic model is based on the Drucker-Prager yield criterion having a confinement-sensitive hardening sub-model. To examine the predictive capacity of the model, it was applied to study a series of laboratory experiments where a number of concrete cylinders were exposed to an active confinement pressure. Furthermore, the model was used in a FE study of concrete-filled steel tubes, in which the state of stress is more complex and the confining stresses on the concrete core are induced by passive confinement provided by the steel tube.

Key words: confined concrete, constitutive modeling, non-linear finite element analyses, concrete-filled steel tube.

1. INTRODUCTION

Concrete in compression is usually characterized with a stress-strain relationship obtained from uniaxial standard compression tests. However, most concrete structural elements are subjected to a multiaxial stress state. A uniaxial stress state represents only one of an infinite number of multiaxial stress conditions to which an element of concrete in a structure may be subjected throughout the loading history of the structure; see Kotsovos (1987). The response of concrete varies widely for different stress states and it is therefore important to know how the concrete behaves for different multiaxial stress states. As an example, Kotsovos shows the variation of the peak axial compressive stress sustained by a concrete cylinder with increasing confining pressure. It was noted that a small confining pressure of about 10 percent of the uniaxial cylinder compressive strength was sufficient to increase the load-bearing capacity of the specimen by as much as 50 percent.

A confinement-sensitive compression model to be used in FE analyses of concrete structures has been developed. Various methods of introducing confinement or pressure dependence have been proposed in the literature. One solution was reported by Malvar *et al.* (1997) where the compressive strength was made dependent on the hydrostatic pressure. Another way of dealing with the problem was suggested by Chen and Han (1987) who defined the plastic modulus as a function of the hydrostatic pressure through a modification factor. However, it is the authors' opinion that in order to simulate the confinement dependence completely it is necessary to make both the strength and the plastic modulus dependent on the confinement. This way of introducing confinement sensitivity in both the strength and the plastic modulus is believed to be a novel feature. Furthermore, it is believed that the hydrostatic pressure is an unfortunate choice of controlling parameter as two different stress situations can share the same hydrostatic pressure.

The proposed model is fundamentally an elasto-plastic model based on flow theory, i.e., it consists of a yield surface, a hardening rule, a yield law and reliance on the assumption of strain decomposition. What makes this model different from conventional elasto-plastic models is its capability to incorporate confinement into the integration of the internal state. It is a well-known fact that the response for a general stress situation cannot be captured with a conventional elasto-plastic model calibrated with only a limited set of strength data. That is, frequently used data for calibration of such models are a uniaxial stress-strain relation together with some factor giving the relation between uniaxial and biaxial compressive strength. With these data at hand, it is explicitly assumed that the hardening rate for all loading histories is the same. This is not the case, as can easily be observed by performing a numerical simulation of a situation outside the calibration data range. Such a simulation will reveal too soft behavior; see Figure 1. To resolve this discrepancy when simulating a general situation calls for a more complete set of material data.

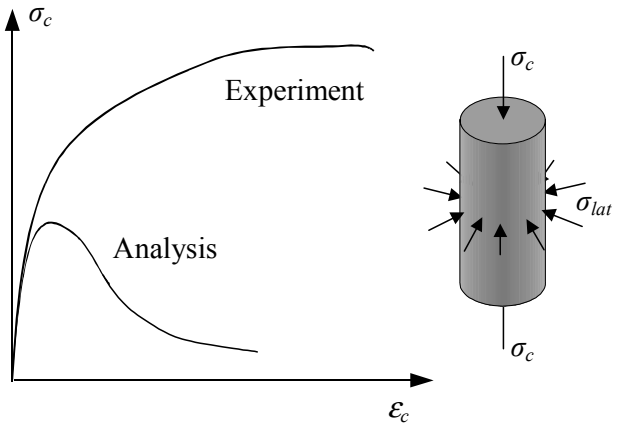

Figure 1 – Typical difference of experimental and analysis result for confined concrete.

The first section of this paper gives a brief description of the fundamental behavior and theories of confined concrete, for the cases of both active and passive confinement. The second section gives a description of the constitutive formulation of the model. Apart from the classical formulation, it consists of a discussion about the concept of confinement-sensitive hardening. Further, the section includes a description of the application of this model and a verification of it. The last section shows an example of an application of the model in a study of concrete-filled steel tubes with some comments on the results. Finally, some remarks and conclusions are presented.

2. CONFINED CONCRETE

2.1 Active confinement of plain concrete

Richart *et al.* (1928) were the first to observe that confined concrete showed greatly increased maximum compressive strength, increased stiffness, and extended strain at which the peak stress was reached; see Figure 2. The concrete can sustain large deformation without substantial reduction of the load-bearing capacity and fails gradually in a ductile way. A number of experimental and theoretical studies on normal-strength concrete subjected to multiaxial states of stress have been performed, for example by Richart *et al.* (1928), Mills and Zimmerman (1970), Pantazopoulou (1995) and Imran and Pantazopoulou (1996). To consider the increased concrete strength due to confinement Richart *et al.* (1928) proposed the well-known empirical formula:

$$f_{cc} = f_{co} + k\sigma_{lat} \tag{1}$$

where f_{cc} is the axial compressive strength of concrete confined by the lateral stress σ_{lat}, f_{co} is the uniaxial compressive strength of the concrete, and k is the so-called triaxial factor and is found to be 4.1. Although newer test results have suggested a modification of this relation, the basic approach for determining the confined strength remains the same. To calculate the axial compressive strain at peak stress ε_{cc} they also proposed the following equation:

$$\varepsilon_{cc} = \varepsilon_{co}\beta_1\left[\frac{f_{cc}}{f_{co}} - \beta_2\right] \tag{2}$$

where ε_{co} is axial compressive strain at peak uniaxial stress, $\beta_1 = 5$ and $\beta_2 = 0.8$. Using equation (1) it can be written as a function of the lateral confining pressure as:

$$\varepsilon_{cc} = \varepsilon_{co}\beta_1\left[\left(1 + \frac{k\sigma_{lat}}{f_{co}}\right) - \beta_2\right] \tag{3}$$

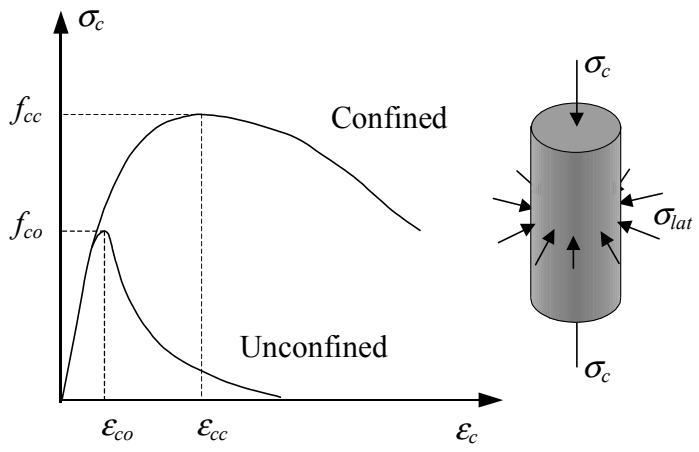

Figure 2 – Schematic stress-strain relations for unconfined and confined concrete.

The experimental data for high-strength concrete under multiaxial states of stress are less extensive than those for normal-strength concrete. However, Attard *et al.* (1996) performed a test series of high-strength concrete subjected to low confining pressure and Ansari and Li (1998) carried out a comprehensive experimental program with high confining pressure, ranging up to $1.0f_{co}$. They found that the influence of confining pressure on the maximum compressive strength of high-strength concrete is not so pronounced as on that of normal-strength concrete. According to Cederwall (1988), can the factor k in equation (1) be assigned a value of 3 to 4 for high-strength concrete.

2.2 Passive confinement in concrete-filled steel tubes

Triaxial stresses in concrete-filled steel tubes have been studied by several researchers, for example Gardner and Jacobson (1967), Tomii *et al.* (1977), Orito *et al.* (1987) and Schneider (1998). In a composite column consisting of a concrete-filled hollow steel section, compressive confining stresses on the concrete core are induced by passive confinement provided by the steel tube. In the case of passive confinement, the confining pressure is not constant as is the case for active confinement, and it also depends on the lateral deformation of the concrete core under axial load and the stress-strain relationship of the confining steel. However, it has been found that the concrete behavior is similar irrespective of whether the confining pressure is active or passive; see Attard *et al.* (1996).

Short concrete-filled steel tubes concentrically loaded on the entire section are significantly affected by the difference between the values of Poisson's ratio of the steel tube, ν_a, and the concrete core, ν_c. In the initial stage of loading, Poisson's ratio of concrete is lower than for steel; therefore, the steel tube expands faster in the radial direction than the concrete core, i.e. the steel does not restrain the concrete core. As the load increases and the compressed concrete starts to plasticize, the lateral deformations of the concrete catch up with those of the steel and, for further increase in load, the steel tube restrains the concrete core and the hoop stresses in the steel become tensile (σ_{ah}). At this stage and later, the concrete core is stressed triaxially and the steel tube biaxially; see Figure 3.

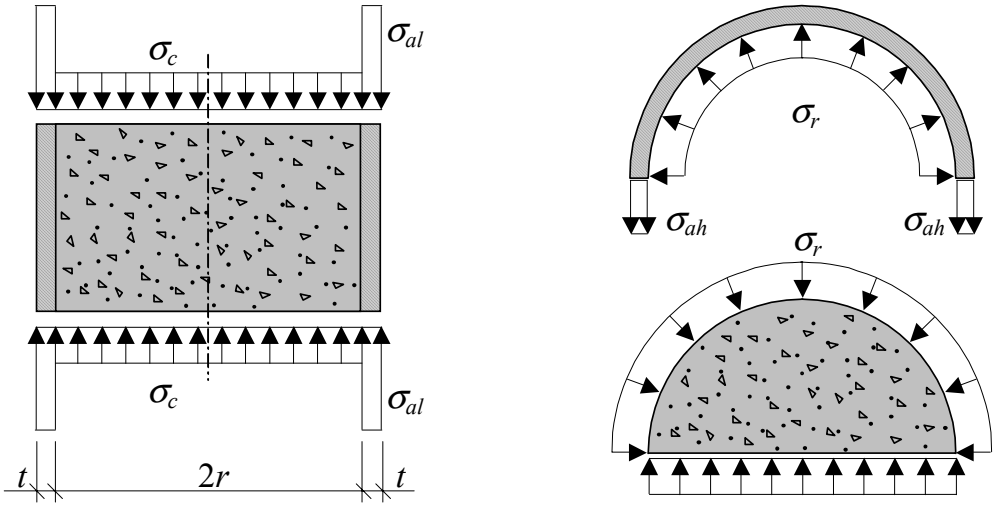

Figure 3 – Stress conditions in the steel tube and the concrete core.

From the equilibrium of the forces acting on the half tube, it is possible to establish a relation between the hoop tensile stresses σ_{ah} and the internal pressure σ_r:

$$\sigma_r = \frac{t}{r}\sigma_{ah} \tag{4}$$

where r and t are the radius and thickness of the steel tube, respectively. By setting $\sigma_{lat} = \sigma_r$ and using equations (1) and (4), the ultimate compressive strength of the concrete core confined by a steel tube can now be calculated as:

$$f_{cc} = f_{co} + k\frac{t}{r}\sigma_{ah} \tag{5}$$

In equation (5) it can be observed that increased hoop tensile stresses in the steel tube give a higher compressive strength of the concrete. However, because of the presence of hoop tension, the steel tube cannot sustain the plastic resistance in the axial direction according to the von Mises yield criterion:

$$\sigma_{ah}^2 + \sigma_{al}\sigma_{ah} + \sigma_{al}^2 = f_y^2 \tag{6}$$

where σ_{al} is the longitudinal compressive stress in the steel and f_y is the yield strength of the steel. This means that when the circumferential tensile steel stress increases due to lateral deformations of the concrete core, the axial compressive steel stress has to decrease.

When the load is applied only to the concrete section, the steel tube has a restraining effect on the concrete core as soon as lateral deformations of the core develop, and the confinement of the concrete core can be most pronounced. In this case, any bond at the steel-concrete interface induces longitudinal compression in the steel tube; i.e. the behavior is influenced by the bond strength. However, when the load is applied to the entire section the bond strength has no or little influence on structural behavior because there is no relative movement between the concrete core and the steel tube.

The total load on the stub column can normally be written as the sum of the contributions from the concrete and the steel:

$$P_{cal} = P_{c,cal} + P_{a,cal} = (f_{co} + k\frac{t}{r}\sigma_{ah})A_c + \sigma_{al}A_a \tag{7}$$

where A_c and A_a are the areas of the concrete core and steel tube, respectively. Assuming that the steel is yielding when the concrete fails, it is possible to find two extreme bounds for the load resistance. The lower bound is obtained by assuming the axial steel stress equal to the yielding stress ($\sigma_{al} = f_y$) and the circumferential steel stress equal to zero ($\sigma_{ah} = 0$). The upper bound, known as the Lohr principle (Lohr 1934), is instead obtained with the steel only acting as an encasement, i.e. setting the axial steel stress equal to zero ($\sigma_{al} = 0$) and the circumferential steel stress equal to the yielding stress ($\sigma_{ah} = f_y$). However, in practice the real situation will be somewhere inbetween and the stress pattern in the structure can be very complex.

3. CONFINEMENT-SENSITIVE CONCRETE COMPRESSION MODEL

3.1 Constitutive formulation

The material model designed for modeling concrete crushing is fundamentally a classical elasto-plastic model, but it is extended to include a confinement-sensitive hardening behavior by means of two adjustment functions connected to the strength and the plastic modulus. The underlying model was chosen as the Drucker-Prager model with associative evolution laws, see Chen and Han (1987). Figure 4 shows the yield surface in the principal stress space. This was a choice guided by the aim of just demonstrating a principle for introducing the confinement sensitivity into the constitutive formulation, but also guided by the fact that the main contributing factor for capturing the confinement sensitivity is given by the hardening rule. That is, the shape of the yield surface only comes into play at onset of yielding and its contribution to the response is not as dominant as the effect of the hardening rule. Another factor affecting the choice of underlying plastic model, though less important, was the ability to produce correct and efficient numerical algorithms for integrating the state. With this model, it is also simple to establish the algorithmic tangent stiffness tensor at a low computational cost, which is a major concern when dealing with implementation issues.

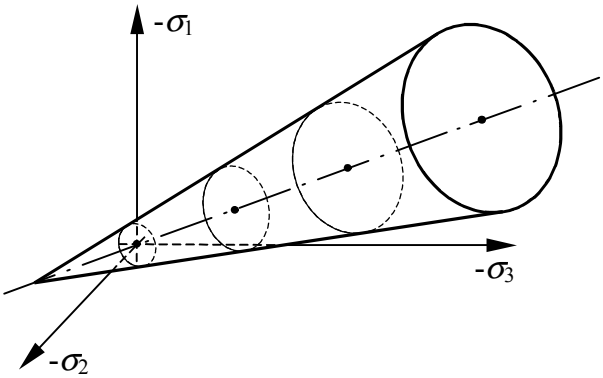

Figure 4 – The Drucker-Prager yield surface in the principal stress space.

The yield surface for the Drucker-Prager model is a linear function in both the deviatoric stress q and the hydrostatic pressure p:

$$F(\boldsymbol{\sigma}, K) = q + p\tan\alpha - K = 0 \tag{8}$$

where K is the strength representing the cohesion and α is the frictional angle. The hydrostatic pressure is defined as:

$$p = -\frac{1}{3}\boldsymbol{\sigma} : \mathbf{I} \tag{9}$$

where $\boldsymbol{\sigma}$ is the stress tensor and $\mathbf{I}$ is the unit tensor. The deviatoric stress is defined as:

$$q = \sqrt{\frac{2}{3}(\mathbf{S} : \mathbf{S})}, \tag{10}$$

where $\mathbf{S}$ is the deviator stress tensor, defined as:

$$\mathbf{S} = \boldsymbol{\sigma} + p\mathbf{I} \,. \tag{11}$$

The next component in the model is the flow rule, expressing the evolution of plastic strains:

$$d\boldsymbol{\varepsilon}^{p} = d\lambda \frac{\partial Q}{\partial \boldsymbol{\sigma}} = d\lambda \frac{\partial F}{\partial \boldsymbol{\sigma}} = d\lambda \left(\sqrt{\frac{3}{2}} \frac{\mathbf{S}}{|\mathbf{S}|} + \frac{\tan\alpha}{3} \boldsymbol{\delta} \right) \tag{12}$$

where $d\lambda$ is the plastic multiplier and $\boldsymbol{\delta}$ is the Kronecker delta. Relation (12) is called the associated flow rule because the plastic flow potential function Q is associated with the yield criterion ($Q = F$); see Chen and Han (1987). Although it is common practice to use a non-associative flow rule ($Q \neq F$) when modeling concrete crushing, again with the aim of investigating a principle, associativity was chosen for the sake of simplicity. The last component of the model, also associative, is the hardening rule, which consists of two parts describing the evolution of the hardening parameter and the strength hardening parameter dependence, i.e.

$$d\kappa = d\lambda \frac{\partial F}{\partial K} = -d\lambda \qquad \text{and} \qquad K = -Hd\lambda \tag{13}$$

where H is the isotropic hardening modulus. Introduction of a confinement dependence on both the hardening parameter and the strength will also make the plastic modulus a function of the confinement. What would be desirable would be to introduce a hyper-surface defined by the three principal stress components and the hardening parameter describing the material strength. This would make it possible to have smooth transitions between different confinement situations. However, this requires that there exists such a surface and from a numerical point of view that it must be reasonably simple in its definition.

It can be argued that a non-associative yield law and a proper yield criterion can be used for achieving the same effect as a confinement-sensitive hardening rule. By just using a non-associative yield law together with a linear yield criterion, the only effect will be a translation of the response curve, keeping the same tendency for different confinement situations. On the other hand, by using a more complex yield criterion in combination with an associative yield law, the dominant effect will simply be a better simulation of onset of crushing. To find the right combination of a non-associative yield law and a complex enough yield criterion seems to be an impossible task; hence, it is a much more straightforward solution to resort to the proposed approach with a confinement-sensitive hardening rule.

The method chosen to introduce the confinement dependence into the hardening sub-model is by means of two adjustment functions f and g. These two functions are defined as polynomials of arbitrary power, i.e.

$$f(\sigma_{lat}) = \sum_{i=0}^{n} a_i \cdot \sigma_{lat}^{i} \tag{14a}$$

$$g(\sigma_{lat}) = \sum_{i=0}^{n} b_i \cdot \sigma_{lat}^{i} \tag{14b}$$

The first function scales the strength K according to the current confinement while the second function scales the hardening parameter κ; see Figure 5. In equations (14a) and (14b) the constants a_i and b_i have to be calibrated from pertinent test data. That is, the confinement influence varies depending on what concrete quality used. With these two adjustment functions, an approximation of the "true" strength hyper-surface is achieved.

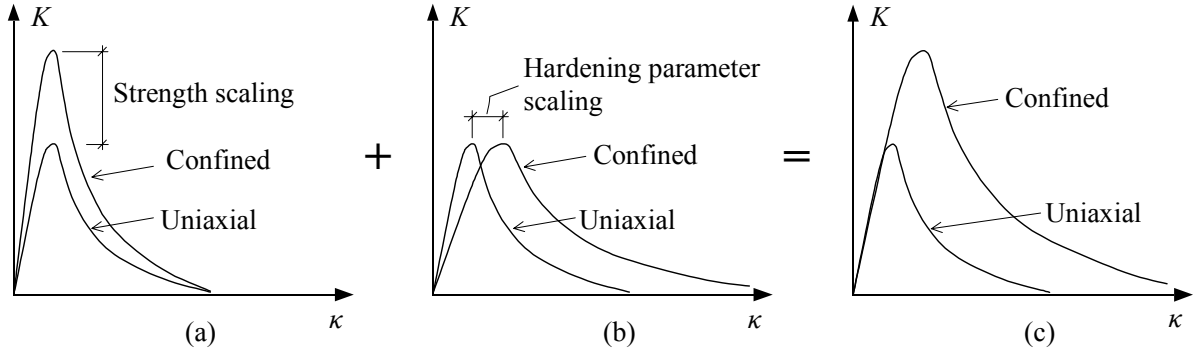

Figure 5 – Strength scaling (a), hardening parameter scaling (b) and resulting confined strength-hardening parameter relation (c).

The confinement value σ_{lat} in an element is taken as the mean value of the two smallest principal stresses under the condition that it is compressive –otherwise it is set equal to zero; see Figure 6. This restriction is due to uncertainties of how the compressive strength is influenced by transverse tensile stresses. Before the model can be extended to include this situation, further experimental investigation has to be done.

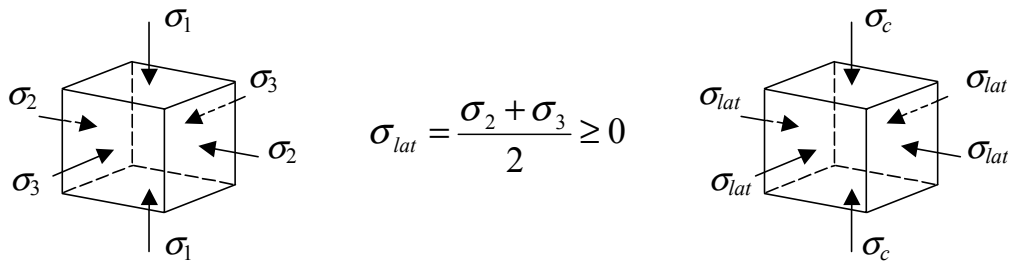

Figure 6 – Definition of stress state in an element when the confinement value is calculated.

To reach a broader public, the model has been implemented in ABAQUS/Standard. Although ABAQUS only offers a Fortran interface for user-defined material models a choice of using the programming language C++ was made; for reference see Lippman (1991). By using C++, it was possible to implement the model in terms of an object-oriented approach, which makes it possible to combine a well-structured code with numerical robustness and efficiency.

3.2 Application and verification

To exemplify the application and verify the confinement-sensitive compression model, an experimental series performed by Imran and Pantazopoulou (1996) was used. In total the experimental series consisted of 130 triaxial tests where the influence of confinement, loading path and moisture content on the stress-strain relation was examined. In this study a part consisting of 42 specimens were chosen to be used in the verification of the material model. The test specimens were of cylindrical shape with a height of 108 mm and a diameter of 54 mm. The peak strength, f_{cc}, and the corresponding strain, ε_{cc}, at given lateral confinement were recorded from the test results and compared with the values calculated according to equations (1) and (3); see Figure 7.

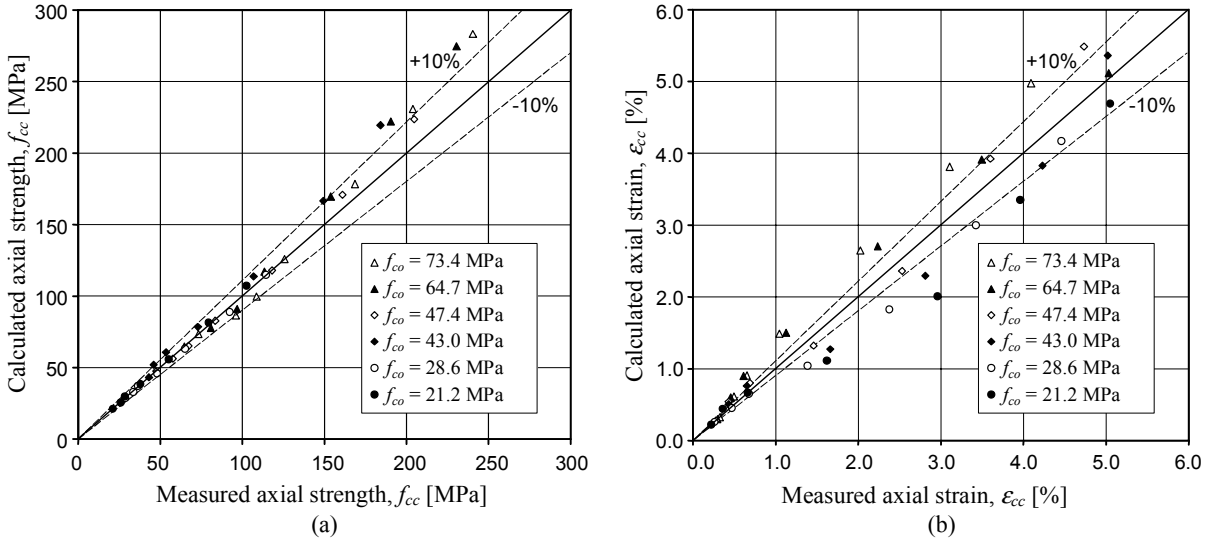

Figure 7 – Comparison of measured and calculated values for (a) the peak strength f_{cc} and (b) the corresponding strain ε_{cc}.

It can be observed that there are rather good agreements between the measured and calculated results for both the strength and the strain. Hence, in absence of triaxial tests it is possible to use the equations in order to derive the two scaling functions used in the material model. However, triaxial tests are more reliable and should be used if possible.

Instead of a relation between stress and strain for the uniaxial behavior, the confinement-sensitive compression model uses a relation between the cohesion and the hardening parameter. The cohesion is calculated as:

$$K = \sigma_c(\varepsilon^p)(1 - \frac{\tan\alpha}{3}) \tag{15}$$

where $\sigma_c(\varepsilon^p)$ is the compressive stress as a function of the plastic strain, ε^p, in the direction of the uniaxial stress. The plastic strain is recalculated into the hardening parameter as:

$$\kappa = \frac{\varepsilon^p}{\left(1 - \frac{\tan\alpha}{3}\right)} \tag{16}$$

The stress-strain relation can be determined by standard uniaxial tests on concrete cylinders. However, it is often not possible to record the stress-strain relation after the maximum strength is reached. Therefore, the post-peak behavior of the concrete can be derived according to the recommendations in CEB-FIP Model Code, CEB-FIP (1993) or CEB Bulletin d'Information 228 (1995). In absence of material tests, the entire stress-strain relation can be derived according to these models. To derive the strength scaling function, $f(\sigma_{lat})$, the peak cohesion, K_{max}, is calculated for a number of values of the lateral confinement, σ_{lat}, according to:

$$K_{\max} = f_{cc}(1-\frac{\tan\alpha}{3}) - \sigma_{lat}(1+\frac{2\tan\alpha}{3}) \tag{17}$$

The function simply describes the increase of cohesion with changes in lateral confinement. Correspondingly, the hardening parameter scaling function, $g(\sigma_{lat})$, is derived from the hardening parameter corresponding to the peak cohesion, κ_{max}, for a given lateral confinement and calculated as:

$$\kappa_{\max} = \frac{f_{cc}(\varepsilon_{cc} - \frac{f_{cc}}{E_c})}{f_{cc}(1-\frac{\tan\alpha}{3}) - \sigma_{lat}(1+\frac{2\tan\alpha}{3})} \tag{18}$$

The values of f_{cc} and ε_{cc} correspond to a specific value of σ_{lat}, and are either taken from triaxial material tests or calculated according to equations (1) and (3), respectively.

To investigate the predictive capacity of the constitutive model in simulating the response under various confinement situations, a set of numerical analyses were carried out simulating the experimental series performed by Imran and Pantazopoulou (1996). Out of this vast material, a test series with $f_{c,cyl}$ = 43.5 MPa was chosen. For this sub-series, seven different levels of confinement were applied. The peak strength, f_{cc}, and the corresponding strain, ε_{cc}, recorded from the seven stress-strain relations obtained in the tests are given in Table 1, and corresponding cohesion and hardening parameters were calculated according to equations (17) and (18).

Table 1 – Investigated experimental series.

Lateral confinement, σ_{lat} [MPa]	Measured		Calculated		FEA	
	f_{cc} [MPa]	ε_{cc} [%]	f_{cc} eq. (1) [MPa]	ε_{cc} eq. (3) [%]	f_{cc} [MPa]	ε_{cc} [%]
0.0	43.1	0.25	43.1	0.25	42.8	0.23
2.2	46.0	0.43	51.9	0.51	50.4	0.46
4.3	53.5	0.65	60.7	0.76	58.5	0.76
8.6	73.0	1.66	78.4	1.27	74.3	1.80
17.2	107.0	2.81	114.0	2.29	105.8	2.81
30.1	149.3	4.23	167.0	3.83	153.0	4.30
43.0	184.2	5.02	219.0	5.36	198.3	5.00

In Figure 8 the obtained values of the cohesion and hardening parameter are plotted against the level of confinement. The values are normalized with respect to maximum values obtained in uniaxial compression, i.e. zero confinement. Also the derived scaling functions for the cohesion and the hardening parameter are shown. Both scaling functions are chosen to be represented by a linear relation. For comparison the results obtained by using equations (1) and (3) to calculate f_{cc} and ε_{cc} are also given in Table 1 and Figure 8.

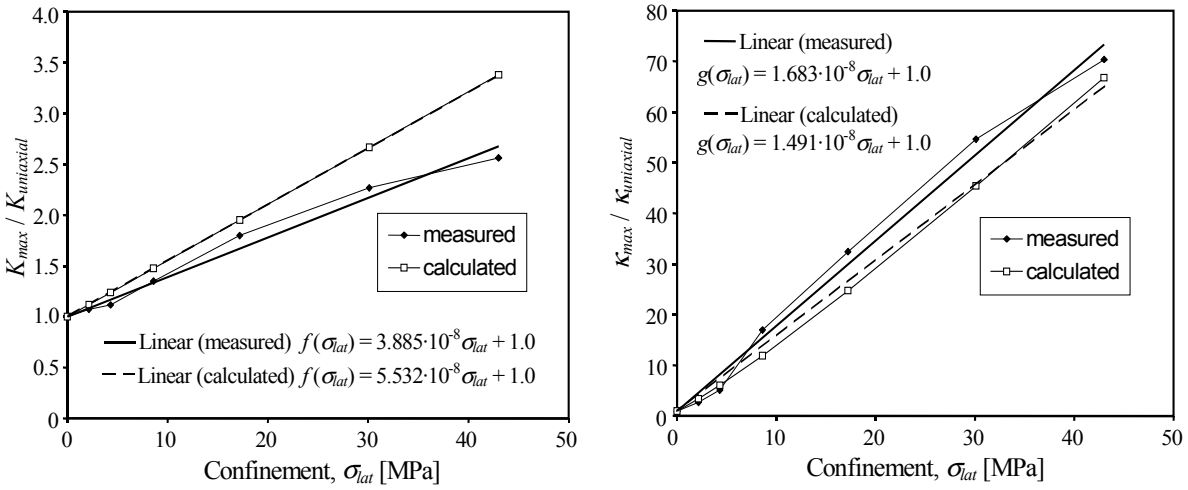

Figure 8 – The normalized values of (a) cohesion and (b) hardening parameter plotted against the level of confinement.

The results from the comparative FE analyses are shown in Figures 9 to 12 where the axial stress is plotted against the total axial strain. The peak strength, f_{cc}, and the corresponding strain, ε_{cc}, obtained in the FE analyses are compared with the test results in Table 1. As can be seen, the correspondence between the numerical results and the experimental data is fairly good. However, this is perhaps not surprising since it is a simple problem regarding both geometry and response.

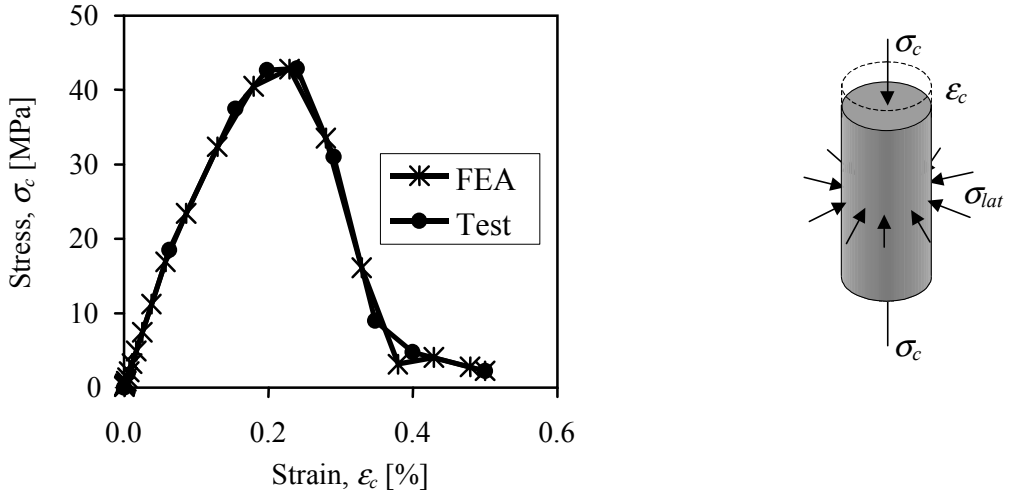

Figure 9 – Results for confinement 0.0 MPa (uniaxial) and the concrete cylinder specimen with a height of 108 mm and a diameter of 54 mm.

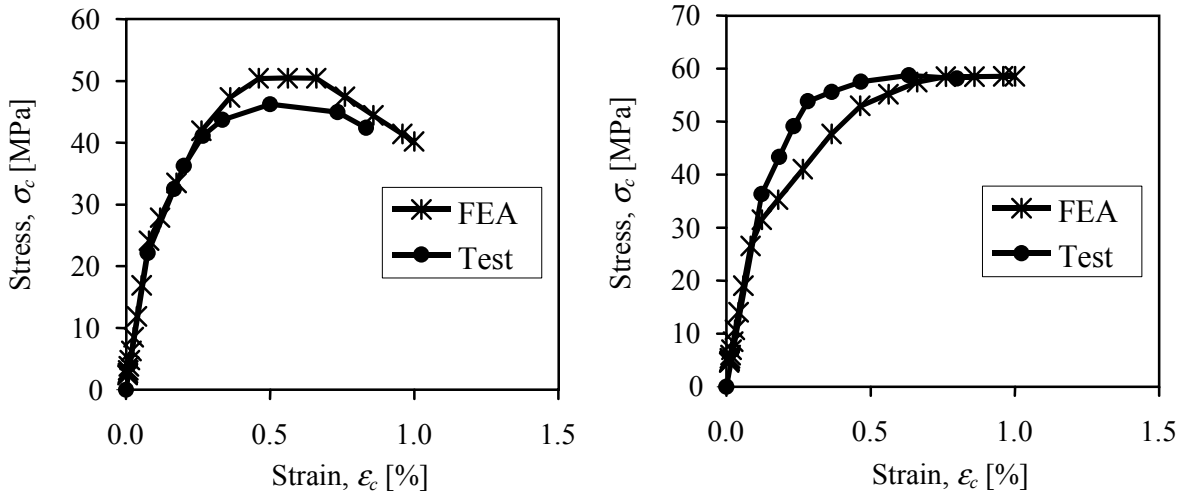

Figure 10 – Results for confinement 2.2 MPa and 4.3 MPa respectively.

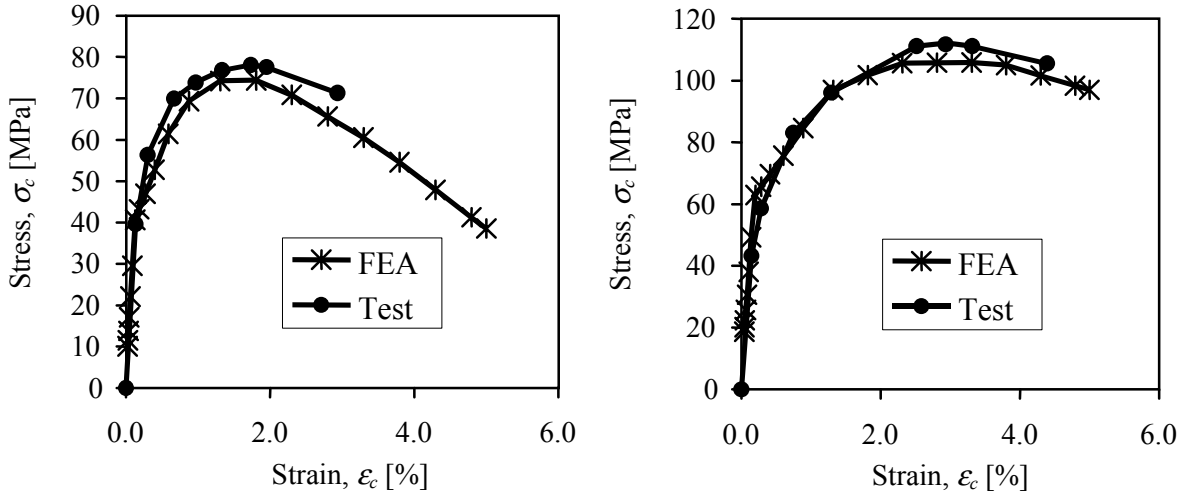

Figure 11 – Results for confinement 8.6 MPa and 17.2 MPa respectively.

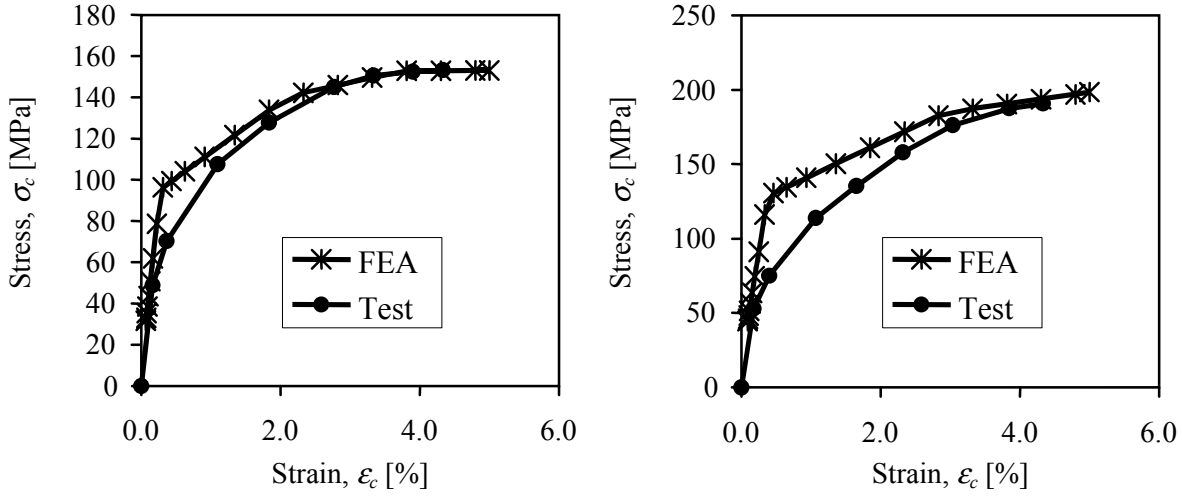

Figure 12 – Results for confinement 30.1 MPa and 43.0 MPa respectively.

4. STUDY OF CONCRETE-FILLED STEEL TUBES

4.1 Experiment

The emphasis of this paper is non-linear finite element analyses and application of the new confinement-sensitive concrete compressive model described in section 3; therefore, the tests are only briefly described. More detailed information about the tests can be found in Johansson (2000). The experimental study consisted of 13 short stub columns with the length of 650 mm and circular cross sections with a 159 mm outer diameter. The thickness of the steel tubes was 4.8 mm. Nine columns were circular hollow steel sections filled with concrete, while four columns, which were to be used as reference columns, were tested unfilled. The load was applied concentrically to the concrete section, to the steel section or to the entire section. Since no effect of increased concrete strength due to confinement is achieved when the load is applied only to the steel section, this loading situation will not be further discussed. The average values of the material properties of the concrete and the steel are summarized in Tables 2 and 3. These values are also used in the following FE analyses.

Table 2 – Material properties of the concrete at the age of 28 days.

$f_{c,cube}$ [MPa]	$f_{c,cyl}$ [MPa]	ε_{co} [‰]	E_c [GPa]	G_F [N/m]
79.4	64.5	3.0	38.5	157

Table 3 – Material properties of the steel.

f_y [MPa]	f_u [MPa]	ε_{ah} [‰]	ε_{au} [‰]	E_a [GPa]
433	568	29	136	206

4.2 Finite element analysis

An established FE model should be able to simulate the columns in a realistic way; such phenomena as the bond between the concrete core and the steel tube, and the increase in concrete compressive strength due to confining effects, have to be taken into account. The non-linear finite element analyses were made with ABAQUS/Standard 5.7; see HKS (1997). Three symmetry planes were used and only one eighth of the column was modeled since the same concentric load was applied in the same way at both ends; see Figure 13. The steel tube, the concrete core and the loading plates had to be separated from each other to simulate the bond between them: therefore they were defined as individual bodies using a three-dimensional finite element model based on solid elements. The confinement-sensitive compression model described in section 3 was used to model the concrete. The uniaxial stress-strain relations in compression, used in the analyses, were derived from standard cylinder tests with concrete from the same batch as the columns; see Table 2. In these tests the stress-strain relation could be recorded only up to the maximum stress. The remaining part of the stress-strain relation was determined in accordance with the CEB Bulletin d'Information 228 (1995). The relation between the cohesion and the hardening parameter was calculated according to equations (15) and (16). The scaling functions for the cohesion and the hardening parameter are represented by linear relations; see Figure 14.

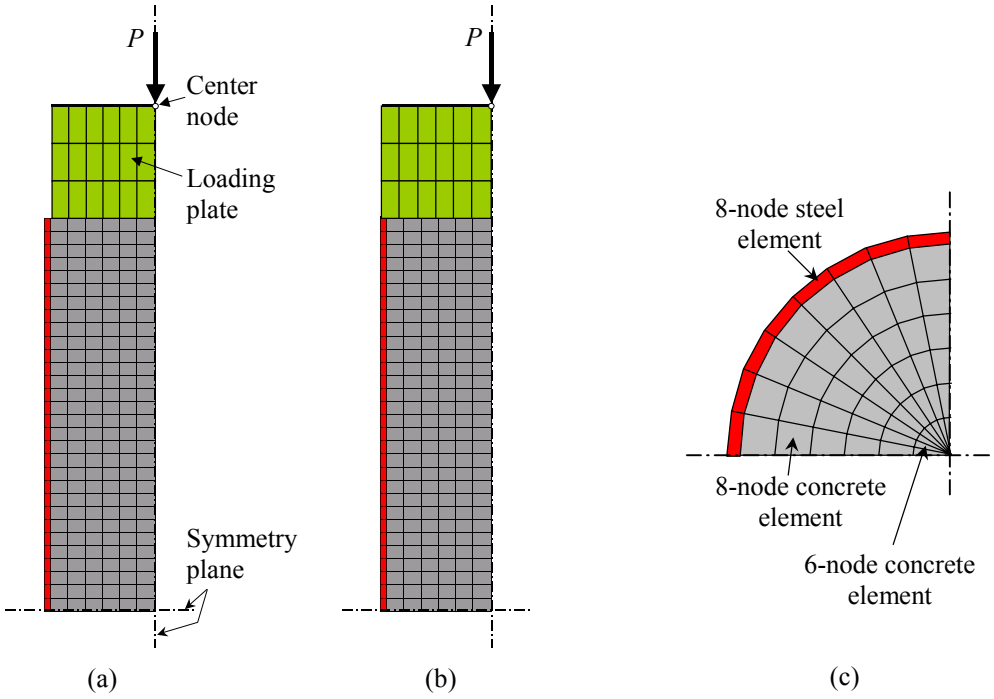

Figure 13 – The FE model: load on (a) concrete section and (b) entire section. The section of the columns in the FE model (c).

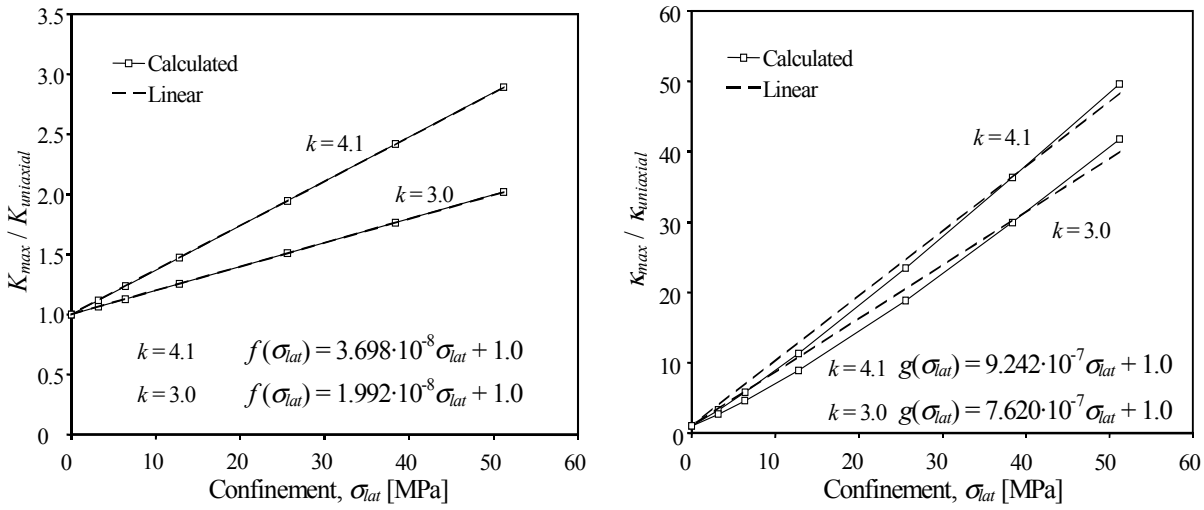

Figure 14 – The normalized values of (a) cohesion and (b) hardening parameter plotted against the level of confinement. (The results for k = 4.1 are shown only for comparison.)

The values for f_{cc} and ε_{cc} were calculated using equations (1) and (3) and corresponding values of K_{max} and κ_{max} according to equations (17) and (18), respectively. The triaxial factor k was set to 3.0 and the friction angle α to 30°. Poisson's ratio for the concrete in the elastic part was approximated as $v_c = 0.2$.

An elastic-plastic model, with the von Mises yield criterion, associated flow rule and isotropic strain hardening, was used to describe the constitutive behavior of the steel; see HKS (1997).

The complete stress-strain relation obtained from uniaxial tensile tests on specimens taken from the steel tubes was used in the FE analyses. Poisson's ratio in the elastic part was set to $v_a = 0.3$. To simulate the bond between the steel tube and the concrete core, surface-based interaction with a contact pressure-overclosure model in the normal direction, and a Coulomb friction model in the directions tangential to the surface, were used. In this way the surfaces could separate and slide relative to each other, as well as transmit contact pressure and shear stresses between the concrete core and the steel tube. According to Baltay and Gjelsvik (1990) the coefficient of friction, μ, between concrete and steel has a value between 0.2 and 0.6. The load was applied as an increased deformation at the center node of the loading plate to model the load of the structure. To distribute the load, all other nodes at the top surface of the loading plate were forced to have the same vertical translation as the center node. The Newton-Raphson iteration method was used to find equilibrium within each load increment. Furthermore, the geometric non-linear behavior, i.e. the local buckling of the steel tube, was taken into consideration.

4.3 Results and discussion

To verify the FE model, a comparison of the load-deformation relationships obtained from tests and those obtained in the FE analyses was made; see Figure 15. When the load was applied only to the concrete section (SFC) the best agreement was obtained when a coefficient of friction of 0.6 was used. Furthermore, as expected for this loading situation, the load resistance increases and the stiffness decreases with a lower value on the coefficient of friction. For the columns with the load applied to the entire section (SFE) a changed value of coefficient of friction did not affect the structural behavior. These observations are also according to what should be expected; see section 2.2. For the SFE column the maximum obtained concrete strength is approximately $1.3f_{c,cyl}$ and for the SFC column it depends on the coefficient of friction and varies from $1.3f_{c,cyl}$ up to $2.2f_{c,cyl}$ when μ is 1.0 and 0.0, respectively. As a further comparison the upper and lower bounds calculated according to equation (7) are shown in Figure 15. It can be observed that the load resistance of all columns falls within these two bounds. In absence of bond strength ($\mu = 0.0$) between the steel and the concrete with the load applied only to the concrete section, there will be no axial stresses ($\sigma_{al} = 0$) in the steel tube and the tube is only used as lateral confinement of the concrete core. Hence, as can also be seen in Figure 15a, this situation corresponds well with the upper bound.

Figure 16 shows how the total axial load is distributed between the steel tube and the concrete core at the midsection of the SFC and SFE columns, when the coefficient of friction is set to 0.6. Although the structural behavior is approximately the same for both the SFE and SFC columns, it can be observed, when comparing the distribution of the axial force during loading, that there are differences in how the load is carried in the columns. In the former, the concrete core and the steel tube are loaded simultaneously; consequently, the load is already distributed from the beginning of the loading; see Figure 16b. In the SFC column, though, the concrete core carries almost the entire load in the initial stage of the loading. As the total load is increased, the concrete core expands in the lateral direction, and contact pressure and shear stresses develop between the concrete and the steel; hence the force carried by the steel tube increases; see Figure 16a. Further, this results in a lower stiffness for the SFC column than for the SFE column where the steel contributes to carrying load from the beginning.

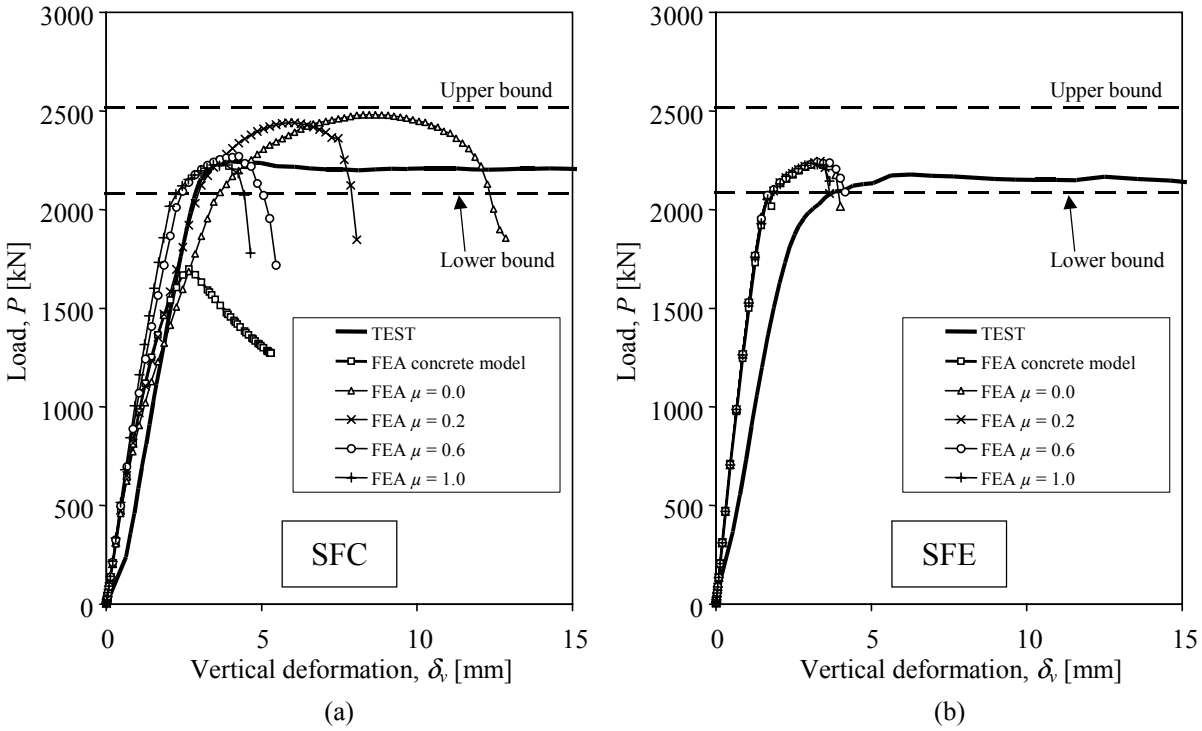

Figure 15 – Comparison of results of FE analyses and tests. Load (a) on concrete section and (b) on entire section.

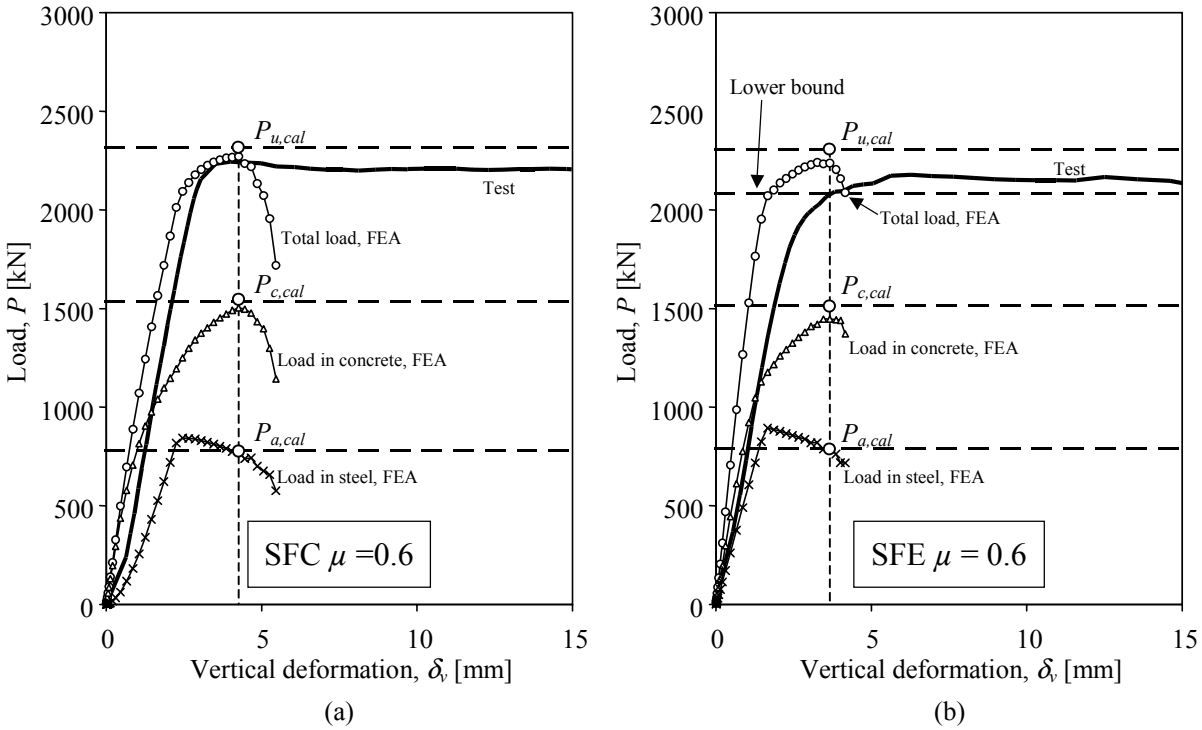

Figure 16 – Distribution of the axial force between concrete and the steel in the midsection of (a) the SFC and (b) the SFE column (μ = 0.6).

Figure 17 shows how the stresses (σ_{al}, σ_{ah} and σ_{at}; see also Figure 18) in a steel element, in the midsection of the SFC and SFE columns, vary during the loading (σ_{at} is the steel stress perpendicular to σ_{al} and σ_{ah}). Also the lateral confinement pressure σ_{lat} is shown, calculated from circumferential steel stress according to equation (5) (observe different scale). First, it can be noticed that the assumption of biaxial state of stress in the steel tube is true, since there is no stress over the thickness of the steel tube, i.e. $\sigma_{at} = 0$. Further, for the SFE column it can clearly be seen that there exists no circumferential steel stress before a vertical deformation of approximately 1.2 mm, when the lateral deformations of the concrete core catch up with those of the steel and a contact pressure is introduced. It can also be observed that because of the presence of circumferential steel stress, the yield strength is not reached in compression; and due to increasing circumferential steel stress, the axial steel stress decreases after the maximum stress is obtained; see Figure 17.

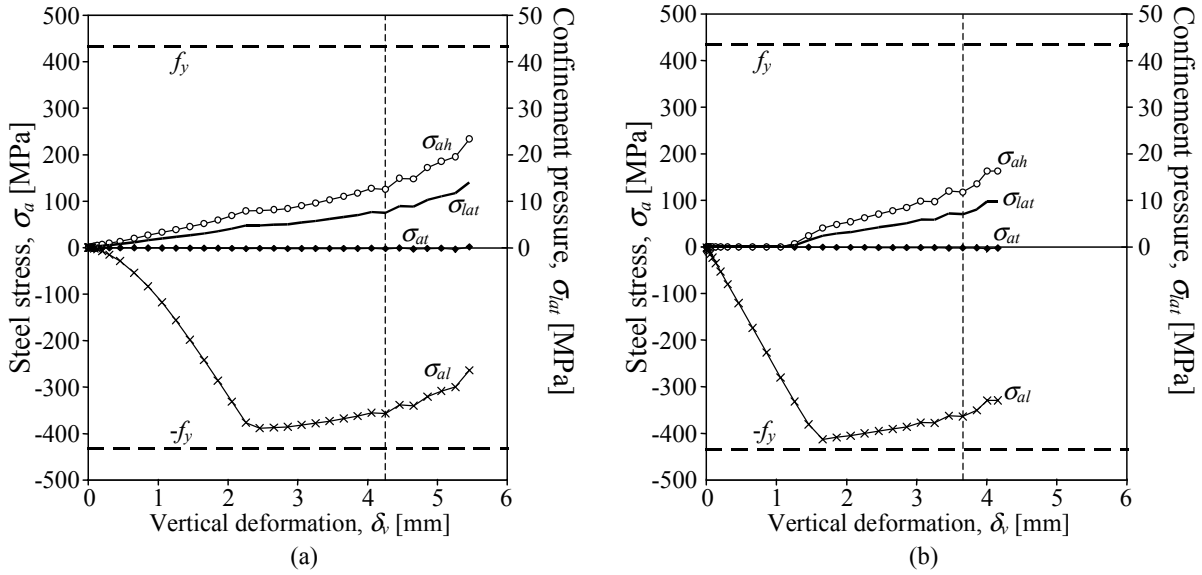

Figure 17 – The stresses for a steel element in the midsection of (a) the SFC and (b) the SFE column (μ = 0.6).

This effect is even more clear in Figure 18 where the stress path for the steel element of the SFC (μ = 0.0, 0.2, 0.6 and 1.0) and SFE columns (μ = 0.6) is shown, i.e. the relation between σ_{al} and σ_{ah}. As long as no hardening of the steel is obtained, this stress path can never go outside of the von Mises yield curve (see equation (6)); consequently the axial compressive steel stress has to decrease when the circumferential tensile steel stress increases. For the SFC column it is possible to see how the coefficient of friction affects the mechanical behavior of the steel tube, by means of the axial to circumferential steel stress ratio. For the higher value (μ = 1.0) the steel tube is mainly subjected to compressive stresses in the axial direction. Meanwhile, in absence of friction (μ = 0.0) only circumferential tensile stresses are present, thus, the steel tube is used only to provide lateral confinement of the concrete core. The latter situation provides the most effective use of the materials; however, it is hard to realize in practical use. For the SFE column, the ratio between axial and circumferential steel stresses is the same independently of the coefficient of friction.

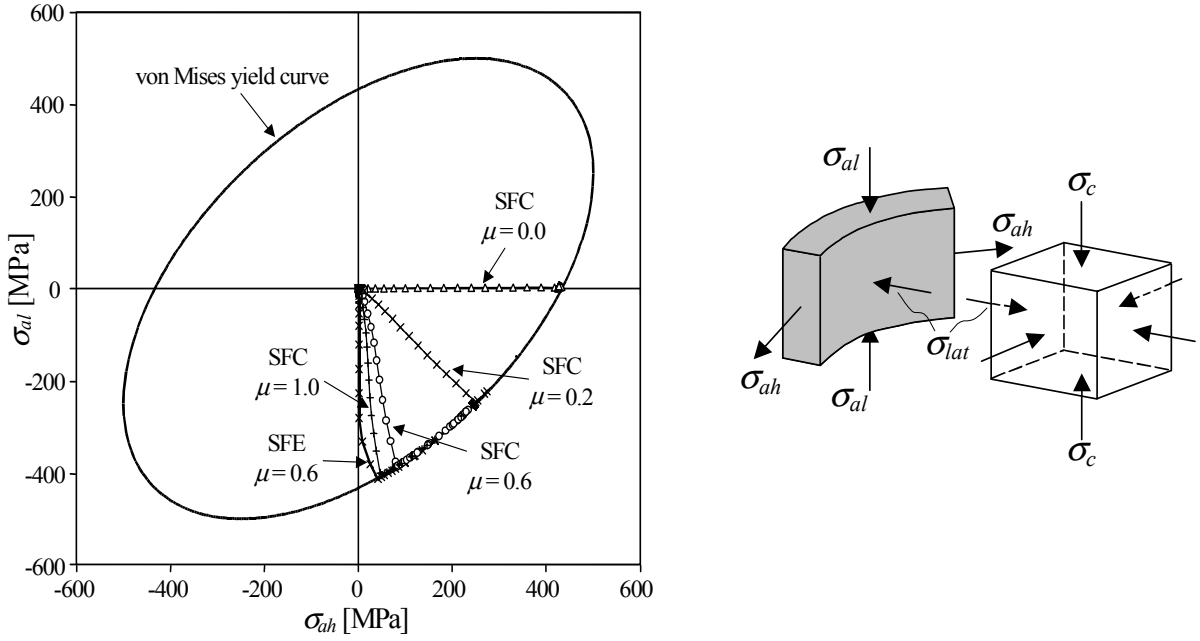

Figure 18 – The stress path for a steel element in the midsection of the SFC (μ = 0.0, 0.2, 0.6 and 1.0) and SFE columns (μ = 0.6).

If the steel stresses (σ_{al} and σ_{ah}) at the ultimate load obtained in the FE analyses (see Figure 17) are used in equation (7), it is possible to calculate the "theoretical" value of the ultimate load resistance $P_{u,cal}$ and its components $P_{a,cal}$ and $P_{c,cal}$. In Figure 16 these values are compared with the results obtained from the FE analyses and it can be seen that there is rather good agreement. However, the problem with using only the theoretical expression still remains, because it is necessary to know the relation between σ_{al} and σ_{ah}, which is hard to find without the FE analyses. This relation depends on the ratio of concrete to steel areas as well as the strength of the two materials. To be able to estimate the resistance and deformation capacity of a concrete-filled steel tube section, it is necessary to know how σ_{al} (i.e. the confinement pressure on the concrete core) and σ_{ah} develops during loading. Therefore, a simple analytical model that takes this into account needs to be developed.

Although the correspondence up to the load resistance between the numerical and experimental results is fairly good, and the structural behavior of the columns is in agreement with theories and previous studies, the post-peak behavior of the columns is not captured satisfactorily. To overcome this problem, not only the strength and hardening parameter needs to be confinement-sensitive; also the shape of the descending branch of the concrete stress-strain relationship should depend on the confinement stress level, i.e. increased confinement should give a more ductile behavior of the concrete; see Figure 2.

5. CONCLUSIONS

An object-oriented implementation of a confinement-sensitive compression model using the programming language C++ was presented. The confinement sensitivity affected both the strength and the hardening parameter and thereby also the plastic modulus. The confinement dependence is introduced by means of two adjustment functions, which can be derived either from triaxial material tests or by the presented theoretical expressions. The applicability of the model was shown in an example. Here results from the model were compared with

experimental data from triaxial compression tests on concrete cylinders exposed to an active confinement pressure. The results showed that the model was capable, in an acceptable way, of reproducing the experimental data.

Furthermore, the model was used in a finite element study of composite columns consisting of concrete-filled steel tubes. There is a rather good correspondence up to the load resistance between the numerical and experimental results. Hence, the model is able to simulate the confining effects on the concrete also when the confining pressure is changing during the load history, i.e. passive confinement. Since the shape of the descending branch of the concrete stress-strain relationship is not confinement-sensitive, the post-peak behavior of the composite columns was not captured adequately. For the columns with the load applied to the entire section, the bond strength did not affect the structural behavior. However, when the load is applied only to the concrete section the load resistance increases and the stiffness decreases with lower bond strength.

6. REFERENCES

Ansari, F. & Li, Q. (1998): "High-Strength Concrete Subjected to Triaxial Compression." *ACI Materials Journal*, Nov.-Dec., Title no. 95-M75, pp. 747-755.

Attard, M. M. & Setung, S. (1996): "Stress-Strain Relationship of Confined and Unconfined Concrete." *ACI Materials Journal*, Sep.-Oct., Title no. 93-M49, pp. 432-442.

Baltay, P. & Gjelsvik, A. (1990): "Coefficient of Friction for Steel on Concrete at High Normal Stress." *Journal of Materials in Civil Engineering*, Vol. 2, No. 1, February, pp. 46-49.

CEB-FIP (1993): *CEB-FIP Model Code 1990, Design Code*. Thomas Telford, Lausanne, Switzerland, May, 437 pp.

CEB Bulletin d'Information 228 (1995): *High Performance Concrete, Recommended Extensions to the Model Code 90, Research Needs*. Lausanne, Switzerland.

Cederwall, K. (1988): "Some Ideas and Studies Concerning the Ultimate Capacity of Composite Steel and Concrete Elements." *Nordic Concrete Journal*, 1988:5, Stockholm, 7 pp.

Chen, W. F. & Han, D. J. 1987: "Plasticity for Structural Engineers." Springer-Verlag, Berlin, Germany, 606 pp.

Gardner, N. J. & Jacobson, E. R. (1967): "Structural Behavior of Concrete Filled Steel Tubes." *ACI Journal*, July, pp. 404-413.

HKS (1997): *ABAQUS/Standard User's Manual, version 5.7*, Hibbit, Karlsson & Sorensen, Inc. Pawtucket.

Imran, I. & Pantazopoulou, S. J. 1996: "Experimental Study of Plain Concrete under Triaxial Stress." *ACI Materials Journal*, Vol. 93, No. 6, pp. 562-573.

Johansson, M. (2000): "Structural Behaviour of Circular Steel-Concrete Composite Columns." Licentiate thesis, Chalmers University of Technology, Div. of Concrete Struct., Göteborg, Sweden.

Kotsovos, M. D. (1987): "Consideration of Triaxial Stress Conditions in Design: A Necessity." *ACI Structural Journal*, May-June, Title no. 84-S29, pp. 266-273.

Lippman, S. B. (1991): *C++ Primer*, *2nd Edition*, Addison-Wesley Publishing Company, reading, USA, 614 pp.

Malvar, L. J., Crawford, J. E., Wesevich, J. W. and Simons, D. (1997): "A Plasticity Concrete Material Model for DYNA3D." *Int. J. Impact Eng*., Elsevier Science Ltd, Great Britain, Vol. 19, pp. 847-873.

Mills, L. L. & Zimmerman, R. M. (1970): "Compressive Strength of Plain Concrete under Multiaxial Loading Conditions." *ACI Journal*, Vol. 67, No.10, Oct., pp. 802-807.

Orito, Y., Sato, T., Tanaka, N. & Watanabe, Y. (1987): "Study on the Unbonded Steel Tube Concrete Structures." *Engineering Foundation Conference on Composite Constructions*, Henniker, New Hampshire, USA, June, 16 pp.

Pantazopoulou, S. J. (1995): "Role of Expansion on Mechanical Behavior of Concrete." *Journal of Structural Engineering*, Vol. 121, No. 12, December, pp. 1795-1805.

Richart, F. E., Brandtzaeg, A. & Brown, R. L. (1928): *A Study of the Failure of Concrete under Combined Compressive Stresses*, Bulletin No. 185, University of Illinois, Engineering Experimental Station, Urbana, Illinois, USA, November, 104 pp.

Schneider, S. P. (1998): "Axially Loaded Concrete-Filled Steel Tubes." *Journal of Structural Engineering*, Vol. 124, No. 10, October, pp. 1125-1138.

Tomii, M. Y., Yoshimura, K. & Morishita, Y. (1977): "Experimental Studies on Concrete Filled Steel Tubular Columns under Concentric Loading." *Proc. Int. Colloquium on Stability of Structures Under Static and Dynamic Loads*, pp. 718-741.